



Cite this: *Phys. Chem. Chem. Phys.*,  
2024, 26, 8210

# Conformational preference of dipeptide zwitterions in aqueous solvents†

Francisco Adasme-Carreño, <sup>\*ab</sup> Alvaro Ochoa-Calle,<sup>\*c</sup> Marcelo Galván <sup>c</sup> and Joel Ireta <sup>\*c</sup>

Proper description of solvent effects is challenging for theoretical methods, particularly if the solute is a zwitterion. Here, a series of theoretical procedures are used to determine the preferred solvated conformations of twelve hydrophobic dipeptides (Leu-Leu, Leu-Phe, Phe-Leu, Ile-Leu, Phe-Phe, Ala-Val, Val-Ala, Ala-Ile, Ile-Ala, Ile-Val, Val-Ile and Val-Val) in the zwitterionic state. First, the accuracy of density functional theory (DFT), combined with different implicit solvent models, for describing zwitterions in aqueous solvent is assessed by comparing the predicted against the experimental glycine tautomerization energy, *i.e.*, the energetic difference between canonical and zwitterionic glycine in aqueous solvents. It is found that among the tested solvation schemes, the charge-asymmetric nonlocally determined local-electric solvation model (CANDLE) predicts an energetic difference in excellent agreement with the experimental value. Next, DFT-CANDLE is used to determine the most favorable solvated conformation for each of the investigated dipeptide zwitterions. The CANDLE-solvated structures are obtained by exploring the conformational space of each dipeptide zwitterion concatenating DFT calculations, in vacuum, with classical molecular dynamics simulations, in explicit solvents, and DFT calculations including explicit water molecules. It is found that the energetically most favorable conformations are similar to those of the dipeptide zwitterions in their respective crystal structures. Such structural agreement is indicative of the DFT-CANDLE accomplishment of the description of solvated zwitterions, and suggests that these biomolecules self-assemble as quasi-rigid objects.

Received 25th November 2023,  
Accepted 5th February 2024

DOI: 10.1039/d3cp05742a

rsc.li/pccp

## 1. Introduction

Under proper conditions, peptides as small as dipeptides (Fig. 1) self-assemble into ordered aggregates of different morphologies like piled layers, tubes, rods, hydrogels, *etc.*<sup>1–3</sup> These aggregates are of great interest due to their resemblance to amyloid-like fibers,<sup>4,5</sup> whose presence in human organs is associated with diseases like Alzheimer's and Parkinson's diseases.<sup>6</sup> Peptide aggregates are also promising candidates for technological applications, owing to their remarkable electrical and mechanical properties.<sup>7–11</sup> Understanding the self-assembly of such systems, at the molecular level,

may thus be valuable for bottom-up design of bionanodevices<sup>10,12</sup> and drug carriers,<sup>13</sup> or for envisaging triggering factors of the amyloid fiber formation.

All hydrophobic natural dipeptides have been crystallized (Fig. 2).<sup>14</sup> Some of these dipeptides crystallize forming pores, and others do it as a set of layers.<sup>14</sup> In these crystals, dipeptides assemble as zwitterions, *i.e.*, with  $\text{NH}^{3+}$  and  $\text{COO}^-$  as the capping groups (Fig. 1). In aqueous solvents, dipeptides prefer

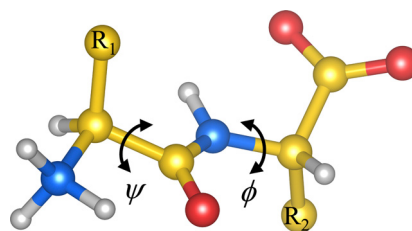


**Fig. 1** Scheme of a dipeptide in the zwitterionic state.  $R_1$  and  $R_2$  stand for side chains 1 and 2, respectively.  $\psi$  and  $\phi$  are dihedral angles denoting the rotation along the indicated covalent bonds. Carbon atoms are shown in yellow, hydrogen atoms in light gray, oxygen atoms in red and nitrogen atoms in blue.

<sup>a</sup> Centro de Investigación de Estudios Avanzados del Maule (CIEAM), Vicerrectoría de Investigación y Postgrado Universidad Católica del Maule, Talca 3480112, Chile. E-mail: fadasme@ucm.cl

<sup>b</sup> Laboratorio de Bioinformática y Química Computacional (LBQC), Departamento de Medicina Traslacional, Facultad de Medicina, Universidad Católica del Maule, Talca 3480112, Chile

<sup>c</sup> Departamento de Química, División de Ciencias Básicas e Ingeniería, Universidad Autónoma Metropolitana-Iztapalapa, Ciudad de México 09340, Mexico. E-mail: aochoagauge@gmail.com, iret@xanum.uam.mx

† Electronic supplementary information (ESI) available. See DOI: <https://doi.org/10.1039/d3cp05742a>



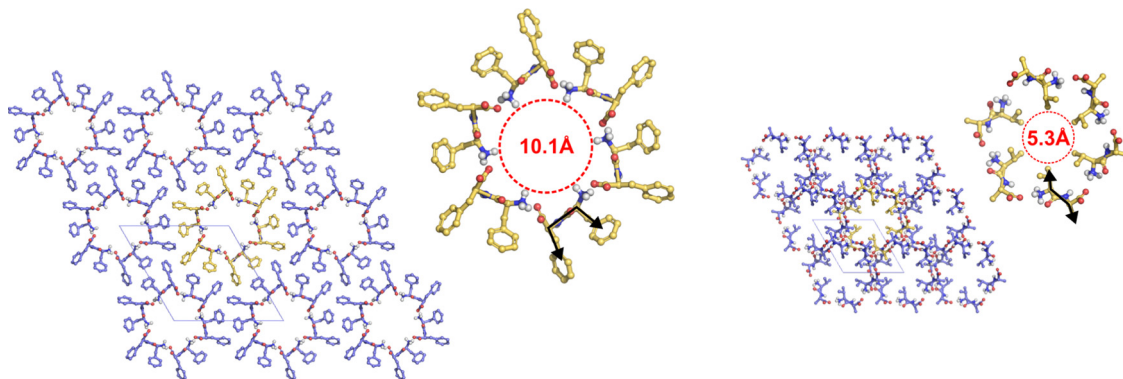


Fig. 2 Arrangement of hydrophobic dipeptides in their crystal structures. Top view of the tubes formed by the F–F (left) and V–A (right) classes with the pore walls delimited by red dashed lines. Black arrows show the orientation of the side chains. Dipeptides with their side chains in *cis* conformation form wide pores ( $\sim 10$  Å diameter). Dipeptides with their side chains in *trans* conformation form narrow pores ( $\sim 5$  Å diameter). Carbon atoms are colored in yellow, oxygen atoms in red, nitrogen atoms in blue, and hydrogen atoms in light gray. Side-chain hydrogen atoms are hidden for visual clarity. Unit cell is shown as thin gray lines.

to be in the zwitterionic state too.<sup>15</sup> Therefore, we would like to get insight into the influence that such locally charged but globally neutral state has on dipeptide conformations, which may be crucial along the self-assembly pathway of these systems. In this work, we use theoretical methods for investigating the influence of the zwitterionic state in the conformational preferences of two sets of hydrophobic natural dipeptides. Both sets of dipeptides crystallize forming pores. The set here named class V–A comprises the Ala-Val (AV), Val-Ala (VA), Ala-Ile (AI), Ile-Ala (IA), Ile-Val (IV), Val-Ile (VI) and Val-Val (VV) dipeptides, and the set labelled as class F–F includes the Phe-Phe (FF), Leu-Leu (LL), Leu-Phe (LF), Phe-Leu (FL) and Ile-Leu (IL). Determining peptide zwitterion conformations in solution is challenging using theoretical methods. This is primarily due to the inadequacy of the procedures commonly used for describing solvent effects, particularly in situations in which the solute is locally or globally charged.

Commonly, the non-zwitterionic *N*-acetyl-alanyl-*N'*-methylamide (Ac-Ala-NHMe) molecule is used to investigate peptide conformational preferences.<sup>16</sup> Ac-Ala-NHMe is a capped peptide comprising two peptide bonds flanking a single side chain; hence, it is usually called dipeptide. The crystallized natural peptides mentioned above, however, are constituted by two amino-acid residues linked by one peptide bond. Thus these are named dipeptides too. Hereinafter the term dipeptide is used solely for referring to the latter systems. Dipeptide conformations are here characterized in terms of the  $\phi$  and  $\psi$  torsional angles (Fig. 1), in the same way as these torsional angles are ordinarily used to describe the Ac-Ala-NHMe conformations.

According to calculated Ramachandran maps for Ac-Ala-NHMe, *i.e.*, plots of its potential energy surface (PES) in terms of  $\phi$  and  $\psi$ , the most stable conformation in aqueous solvent is the so-called polyproline II conformation,<sup>17–22</sup> outcome that has been confirmed using Raman optical activity experiments.<sup>23</sup> If Ac-Ala-NHMe is considered to be in vacuum, the preferred conformation is predicted to be an extended one,<sup>24,25</sup> a

geometry similar to that of protein residues in strands forming  $\beta$ -sheets.<sup>26</sup> The  $\beta$ -sheets are common protein backbone conformations characterized by  $\phi$ ,  $\psi$  mean values around  $-130^\circ$ ,  $144^\circ$  in antiparallel  $\beta$ -sheets and  $-122^\circ$ ,  $137^\circ$  in parallel  $\beta$ -sheets, respectively.<sup>27</sup> Thus, either in aqueous solvent or in vacuum, Ac-Ala-NHMe prefers to adopt conformations that lie in the upper left quarter of the Ramachandran map (Fig. 3).<sup>28</sup> Molecules containing glycine (Gly) instead of Ala behave similarly.<sup>15,29</sup> The conformations of class V–A dipeptides in crystals grown in aqueous solutions are similar to those of a  $\beta$ -strand segment (Fig. 3). These conformations are characterized by  $\phi$ ,  $\psi$  dihedral angles with values around  $-137^\circ$  and  $155^\circ$ , respectively.<sup>30</sup> However, conformations of class F–F dipeptides in their crystals are quite different from those of the class V–A (Fig. 3). Conformations of class F–F dipeptides lie in the upper right quarter of the Ramachandran map and are

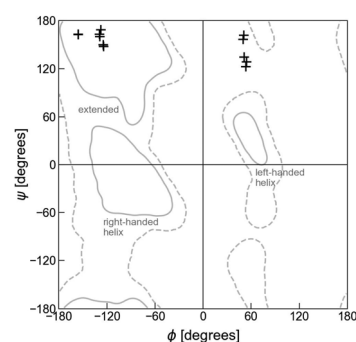


Fig. 3 Ramachandran plot and dipeptide conformations in the crystals. The + symbols at the upper left quarter correspond to the V–A class conformations in the crystals (side chains in *trans* orientation). The + symbols at the upper right quarter correspond to the F–F class conformations in the crystals (side chains in *cis* orientation). Solid lines account for the 95% of residue conformations in protein crystals, and dashed lines for 99%.<sup>31</sup> Apart from the extended conformations, that usually form part of  $\beta$ -sheets and polyproline II motifs, regions in which residue conformations correspond to right- and left-handed helices, other major backbone motifs of proteins, are also indicated.



characterized by a  $\phi$  angle around  $60^\circ$ , and a  $\psi$  angle with values between  $120^\circ$  and  $170^\circ$  (Fig. 3).<sup>30</sup>

Despite the conformational differences described above, both classes of dipeptides, the F-F and V-A, crystallize as a bundle of tubes in aqueous solutions.<sup>32,33</sup> In such crystal structures, however, class V-A dipeptides accommodate their side chains in a *trans* arrangement, while the class F-F dipeptides do it in a *cis* conformation, with respect to the peptide plane (Fig. 2). Consequently, the interior of the formed tubes is hydrophobic and narrow in class V-A crystals, whereas hydrophilic and wide in the class F-F ones. These crystal morphologies seem to be dictated by inter- and intra-peptide interactions, as well as by interactions with the solvent.<sup>34–37</sup>

For example, if the FF crystal is grown in methanol or tetrahydrofuran instead of water, the crystal structure changes as well as the FF conformation in it, which becomes similar to an extended one, like the arrangement of amino-acid residues in strand-forming  $\beta$ -sheets.<sup>35,37</sup>

To determine the conformational preferences of dipeptide zwitterions in aqueous solvent, we use density functional theory (DFT) calculations and classical molecular dynamics (MD) simulations, combined with explicit and implicit solvent models. As mentioned above, proper description of solvent effects is challenging for theoretical methods. Particularly if the solute is a zwitterion, since it is a neutral molecule possessing both positive and negative electrical charges. Therefore, care should be taken in selecting the solvent model for investigating such kinds of systems. If an implicit solvent model is chosen, it should describe equally well both the cationic and anionic environments coexisting in the same molecule. The latter is not the case for commonly used implicit solvent models.<sup>38</sup> If an explicit solvent model is used, it should be considered that a minimum number of water molecules is required to stabilize the zwitterionic state of a peptide.<sup>39,40</sup> Inclusion of explicit solvent in DFT calculations has been mostly done for investigating microsolvation effects on the conformation of peptides and their relative stability at 0 K.<sup>27,41,42</sup> Implicit solvent models, however, can be used to estimate relative stabilities at room temperature, as these models are usually parameterized to estimate free energies. Here we use both solvent models together with DFT calculations to determine the optimal conformation of the zwitterions in solvent and implicit solvent to determine relative stabilities at room temperature.

To choose a suitable implicit solvent model that adequately describes solvated dipeptide zwitterions, we first investigate the tautomerization reaction of Gly (Fig. 4). It is found that among the different implicit solvation models tested, the charge-asymmetric nonlocal determined local-electric (CANDLE) solvation model<sup>43</sup> gives the best result for the free energy difference between the canonical and the zwitterionic state of Gly, as compared to the experimental value. Thus, geometries obtained for each dipeptide zwitterion, obtained combining MD simulations and DFT calculations, are solvated using CANDLE. In this manner, it is found that the most favorable conformation for dipeptide zwitterions in aqueous solution is quite similar to the

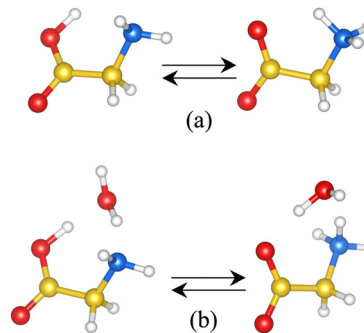


Fig. 4 Glycine tautomerization reaction of (a) the non-assisted model and (b) the assisted model.

conformation of the dipeptide in the corresponding crystal structure, and that the zwitterion–solvent interaction is fundamental in determining the preferred conformation of, primarily, the class F-F dipeptides. Furthermore, it is also found that the conventional continuum solvation model such as the integral equation formalism of the polarizable continuum model (PCM)<sup>44–46</sup> predicts that only the V-A class dipeptides adopt conformations like these in their respective crystal structures. Lastly, it is argued that the obtained results help to understand the self-assembly mechanism of the investigated systems.

## 2. Methodology

### 2.1. Glycine tautomerization reaction

To select an adequate solvent model for describing solvated zwitterions, the energy associated with the Gly tautomerization reaction,  $\Delta E_{\text{tot}}$  (Fig. 4), is calculated at the DFT level of theory using the Perdew–Burke–Ernzerhof (PBE) approximation<sup>47</sup> to the exchange–correlation functional, and the Grimme's D2 dispersion corrections.<sup>48</sup> Several solvation models are tested: conventional continuum solvation models like PCM and the self-consistent reaction field solvation model (SMD),<sup>49</sup> the self-consistent solvation models within the joint-density functional theory (JDFT),<sup>50</sup> such as the PCM-like model proposed by Gunceler, Letchworth-Weaver, Sundararaman, Schwarz and Arias (GLSSA13),<sup>51</sup> the spherically averaged liquid susceptibility ansatz (SaLSA),<sup>52</sup> and CANDLE, a solvation model derived from SaLSA. The solvent is also described using classical DFT (CDFT) for fluids with a simplified free energy functional for liquid water.<sup>53</sup> PCM and SMD are tested using the Gaussian 09 software<sup>54</sup> with a 6-311+G(d,p) basis set. The other solvent models are used as implemented in the JDFTx code<sup>55</sup> version 1.6.0, with the Garrity–Bennett–Vanderbilt library of ultrasoft pseudopotentials<sup>56</sup> and a plane-waves basis set with an energy cutoff of 800 eV.

### 2.2. Searching the lowest energy conformations for dipeptide zwitterions in aqueous solvent

The conformational space of the investigated dipeptides in the canonical state, *i.e.*, with  $-\text{NH}_2$  and  $-\text{COOH}$  as capping groups,



is explored to identify the allowed conformations in vacuum. The canonical state is used in this point of the study because it is known that the zwitterionic state is not stable in vacuum. The PES as a function of the torsion angles  $\phi$  and  $\psi$  (Fig. 1) is calculated using PBE and the dispersion correction method reported by Tkatchenko and Scheffler (TS),<sup>57</sup> as PBE-TS has been shown to properly describe peptide systems.<sup>11,30,58</sup> Plane waves and pseudopotentials together with the projector augmented-wave method<sup>59,60</sup> are used with an energy cutoff of 1100 eV. The dipeptide in vacuum is modeled using the supercell approach, where the unit cell is chosen large enough to avoid interactions with neighboring images. The  $\Gamma$ -point is employed for sampling the Brillouin zone. These DFT calculations are carried out with the Vienna *ab initio* simulation package (VASP).<sup>60,61</sup>

The PES maps are obtained varying the torsion angles  $\phi$  and  $\psi$  from  $-180^\circ$  to  $180^\circ$  in twelve steps of  $30^\circ$  each, yielding a total of 144 distinct geometries. The latter are subjected to geometry optimization using the RMM-DIIS algorithm<sup>62</sup> (or the conjugate gradient algorithm upon convergence issues) with a convergence criterion of a maximum force of  $1.2 \times 10^{-2}$  eV  $\text{\AA}^{-1}$ . The atoms defining  $\phi$  and  $\psi$  are fixed and the others fully optimized. The positions for the fixed atoms are chosen such that bond distances and angles associated with them equal those of the optimal geometry of the fully extended conformation in vacuum. The optimal orientation of the carboxyl capping group is only evaluated for the FF dipeptide varying the N-C-C-O dihedral angle. The  $-\text{COOH}$  orientation with the lowest energy for each  $(\phi, \psi)$  pair in FF is used in the initial geometry for all the other dipeptides. The full PES maps are generated using a cubic spline interpolation.

The structures connected to the minima thus obtained are further relaxed without constraints. Afterwards, these optimized canonical dipeptides are turned into zwitterions, solvated with explicit water molecules by inserting them into a pre-equilibrated cubic box of water molecules with a padding of 10  $\text{\AA}$ . For this the VMD software is used.<sup>63</sup> The solvent is fully relaxed around the dipeptides using a classical MD equilibration protocol. The water molecules are first energetically minimized by 20 000 steps using the conjugate gradient and line search algorithm. The CHARMM36 force field<sup>64</sup> with the CMAP correction is used to describe the dipeptides together with the TIP3P water model.<sup>65</sup> The particle mesh Ewald algorithm<sup>66</sup> is chosen to treat the electrostatic interactions under periodic boundary conditions, and the van der Waals forces are smoothly switched off between 9 and 10  $\text{\AA}$ . The minimization is followed by two 100 ps NVT and 500 ps NPT MD simulations. A 2 fs integration time step is used with the water covalent bonds restrained by the SETTLE algorithm.<sup>67</sup> The r-RESPA algorithm<sup>68</sup> is used to integrate the equations of motion, with non-bonded short-range forces computed every time step and a full electrostatic evaluation every five time-steps. The temperature is kept at 300 K using a Langevin thermostat with a damping coefficient of 2 ps<sup>-1</sup>. Pressure is kept at 1 atm by the Nose-Hoover Langevin piston method,<sup>69,70</sup> with an oscillation period of 400 fs and a damping timescale of

300 fs. The dipeptide atoms are fixed at the initial coordinates. These calculations are performed using the NAMD v2.14 software.<sup>71</sup>

A single frame from the trajectory is selected for each dipeptide such that the backbone hydrogen bond (H-bond) acceptors and donors form an expected minimum number of hydrogen bonds; *i.e.*, 3 for  $-\text{NH}^{3+}$  cap, 6 for  $-\text{COO}^-$  cap, 2 for backbone  $-\text{CO}$ , and 1 for backbone  $-\text{NH}$ . Water molecules that do not interact with the dipeptide are removed. The micro-solvated geometries are then geometry optimized with PBE-TS, first with the dipeptide atoms fixed to optimize the orientation of the water molecules, and next fully optimizing all the atomic coordinates. These calculations are carried out using VASP with the same parameters as those used in the PES calculations.

Finally, the optimized geometries for the micro-solvated dipeptide zwitterions are solvated with the implicit solvent models CANDLE and PCM, and fully geometry optimized under each scheme. As is shown below, CANDLE is chosen owing to the adequate description of the Gly tautomerization reaction. PCM is also chosen for contrasting the CANDLE results against a commonly used solvation scheme. In this latter step micro-solvation water molecules are not considered.

## 3. Results and discussion

### 3.1. Glycine tautomerization reaction

In aqueous solution, the canonical and zwitterionic Gly states coexist in chemical equilibrium. Measurements of the corresponding tautomerization free energy,  $\Delta G$ , indicate that the zwitterionic state is more stable by 7.3 kcal mol<sup>-1</sup> than the canonical one at a temperature of 298 K.<sup>72,73</sup> These experimental results opened a theoretical discussion about the number of water molecules needed to stabilize the otherwise unstable Gly zwitterion,<sup>74-76</sup> and whether implicit solvent models are able to stabilize the zwitterion over the canonical state. It has been suggested that an explicit water molecule should be added for predicting  $\Delta G$  values close to the experimental one with implicit solvent models.<sup>77</sup>

Starting from the geometries reported in ref. 77, we calculate the relative stability of zwitterionic Gly with respect to the canonical one, using the solvent models mentioned in the methodology section and two models for representing the solute: the non-assisted model (NAM), in which the solute is the bare Gly, and the assisted-model (AM) in which the solute is Gly plus a water molecule. Both, the canonical and zwitterionic Gly conformations here investigated are such that all heavy atoms lay in the same plane (Fig. 4). In the canonical glycine, the  $-\text{OH}$  group lays in the same plane as the heavy atoms, and it is located such that it can form a hydrogen bond with the  $-\text{NH}_2$  group (Fig. 4(a)). In the AM, the water molecule is located between the amine and carboxylate groups such that it forms hydrogen bonds with both groups either in the canonical and in the zwitterionic state (Fig. 4(b)). The solvated canonical and zwitterionic AM and NAM are fully optimized using each of the solvation schemes.





**Table 1** Glycine tautomerization energy,  $\Delta E_{\text{tot}}$  (in kcal mol<sup>-1</sup>), calculated with different solvation models and using non-assisted (NAM) and assisted models (AM) for representing the solute

Solvation model	$\Delta E_{\text{tot}}$	
	NAM	AM
PCM	1.22	-0.96
SMD	-4.62	-6.34
GLSSA13	-3.36	-4.72
CANDLE		-7.77
SaLSA	-2.28	-3.41
CDFT	-4.72	-5.62
sp-GLSSA13 <sup>a</sup>	-4.90	-5.89
sp-CANDLE <sup>a</sup>	-7.31	-7.86
sp-CDFT <sup>a</sup>	-4.90	-5.89
Exp. <sup>b</sup>	-7.30	

<sup>a</sup> Single point calculation using the PCM geometry. <sup>b</sup> From ref. 72 and 73.

According to the results for  $\Delta E_{\text{tot}}$  listed in Table 1, all the solvation schemes predict the zwitterionic Gly as the energetically favorable tautomer in solution, either with NAM or AM. Except for PCM which only in combination with the AM forecasts the expected ordering. We compare  $\Delta E_{\text{tot}}$  directly against the experimental free energies as the implicit solvation schemes here used were parameterized to predict free solvation energies. Notably,  $\Delta E_{\text{tot}}$  calculated with CANDLE and the AM differ by less than 1 kcal mol<sup>-1</sup> from the experimental tautomerization free energy, and CANDLE in combination with NAM predicts that only the zwitterionic state exists in aqueous solvent. Hence, to be able to calculate  $\Delta E_{\text{tot}}$  with CANDLE and the NAM we perform single-point calculations combining the PCM-optimized geometries with CANDLE. The latter is also done using the GLSSA13 and CDFT solvation schemes. Unexpectedly, all but one of the  $\Delta E_{\text{tot}}$  values calculated in this manner are in better agreement with the experimental value; e.g., we get a difference between experiment and theory of less than 0.1 kcal mol<sup>-1</sup> solvating with CANDLE the PCM-optimized NAM. Nevertheless, the PCM-optimized NAM, solvated with the other solvation schemes, still underestimates the experimental value (in absolute value) by  $\sim 2.5$  kcal mol<sup>-1</sup> (34%) or more. Conversely, all the solvation schemes improve the estimation of the tautomerization energy if the AM is used instead of the NAM. Except for CANDLE in combination with the PCM-optimized geometries. Yet, CANDLE together with the AM provides a better estimation of the tautomerization energy than the other solvation schemes combined with the AM. The appropriate performance of CANDLE is related to the fact that it is calibrated to describe solvation free energies at 298 K of negative and positive species with the same accuracy. For calibrating the CANDLE parameters a set of 346 free energies (240 of neutral molecules, 54 of cations and 55 of anions) obtained at 298 K was used, as reported in ref. 43, 78 and 79. Accordingly, for investigating the most stable conformation of the V-A and F-F dipeptides in aqueous solvent, we use PCM-optimized NAM geometries solvated with CANDLE, and further re-optimized under the CANDLE solvation scheme. The energies thus obtained are used for the conformational ordering

described below. For comparison purposes we also report the energetic analysis obtained with PCM and the NAM, as PCM is a commonly used implicit solvation model.

### 3.2. Conformational search in vacuum

To determine the most stable conformations for the V-A and F-F classes of dipeptide zwitterions in solution, we first explore the conformational space for the corresponding canonical dipeptides in vacuum. For this, we calculate a PES in terms of  $(\phi, \psi)$  for each of the investigated dipeptides using DFT-PBE/TS. These Ramachandran-like maps exhibit well-defined minima labelled according to the corresponding orientations of the side chains (either *cis* or *trans* with respect to the peptide bond plane), as shown in Fig. 5. The regions of low energy somewhat agree with the most-populated Ramachandran regions in proteins (gray lines), but the shape and location differ significantly, likely due to the structural differences among protein residues and the dipeptides studied here; i.e., a protein residue is more like Ac-Ala-NHMe. Dipeptide structures associated with the minima labelled as *t* and *c*, are similar to the *trans* and *cis* dipeptide conformations observed in their crystal structures. The  $(\phi, \psi)$  angles corresponding to the actual dipeptide conformations in these crystals are marked by + symbols in the maps. As can be seen in Fig. 5, all the + marks lay inside the energy basins labelled with *t* or *c*, and in some cases the marks are at the basin minimum. The *t* minima are in the region that is associated with extended conformations such as  $\beta$  sheets in proteins. In contrast, the *c* minima are located in an area that is scarcely populated by protein residues and even considered to be an energetically prohibited region for a hard-spheres model of Ac-Ala-NHMe.<sup>80</sup> For all the dipeptides at least two other well defined minima are found, in one of them dipeptides have their side chains in *cis* conformation (minima labelled as *c'*), and in the others in *trans* conformation (minima labelled as *t'* or *t''* if a fifth minimum exist). The *t''* minima are shallow and appears only for AI, AV, FF and FL. Basins associated with the *c'* minima are close to the Ramachandran region connected to right-handed  $\alpha$ -helices in proteins, and those associated with the *t'* minima of the V-A dipeptide class to the left-handed  $\alpha$ -helices. However, the corresponding basins to *t'* and *t''* minima for the F-F class are in a region poorly populated in protein Ramachandran maps.

The chart in Fig. 6 shows the relative energies for the conformations connected to the minimum at each basin. These relative energies are referred with respect to the lowest one. All the lowest energy conformations of the V-A class dipeptides in vacuum belong to *t* basins, except for the V-A dipeptide whose lowest energy conformation is located in the corresponding *c'* basin (Fig. 6). On the contrary, the lowest energy conformations of the F-F class belong to *c'* basins, except for the IL dipeptide whose lowest energy conformation is located in the corresponding *t* basin. Notably, the energy difference between the *t* and the *c'* minima is around 1 to 3 kcal mol<sup>-1</sup> for all these canonical dipeptides in vacuum. Nevertheless, none of these dipeptides crystallize adopting a conformation connected to a *c'* basin. In Fig. 6 are also depicted the relative



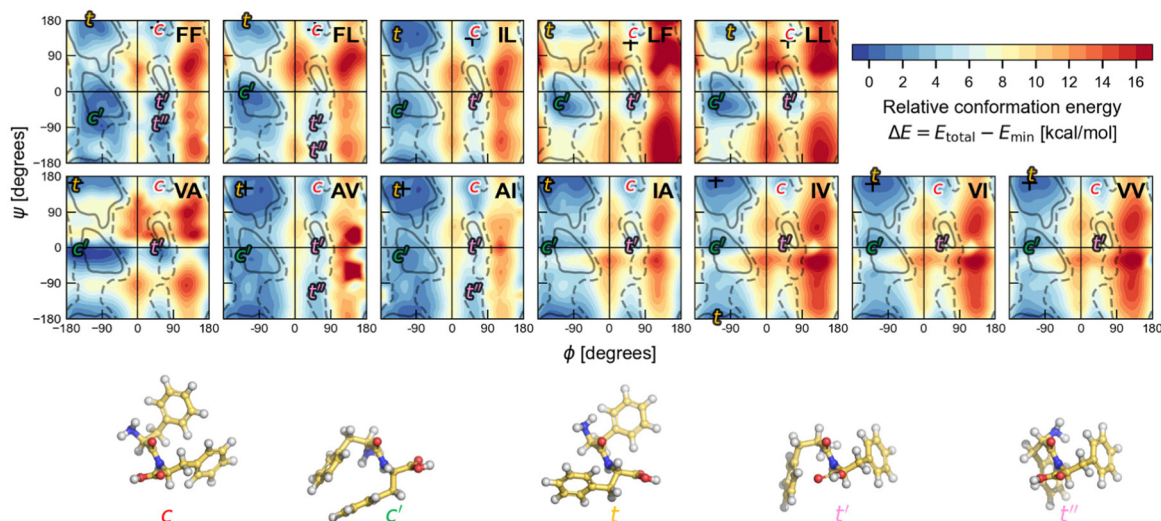


**Fig. 5** Ramachandran PES of each the twelve investigated dipeptides in vacuum. Relative energies are referred to the lowest minimum at each PES. + symbols indicate the conformation observed in the corresponding crystals. The minimum position at each basin is labelled with *t* (in yellow) if the relative side chain orientation is *trans*, or with *c* (in red) if such orientation is *cis*. The labels *c'* (in green), *t'* and *t''* (both in pink) stand for minima connected to alternative *cis* and *trans* conformations not observed in dipeptide crystals. Solid lines account for 95% of proteins, and dashed lines for 99%.<sup>31</sup> FF geometries at each of the minima found in the corresponding PES are shown at the bottom. Carbon atoms are colored in yellow, oxygen atoms in red, nitrogen atoms in blue, and hydrogen atoms in light gray.

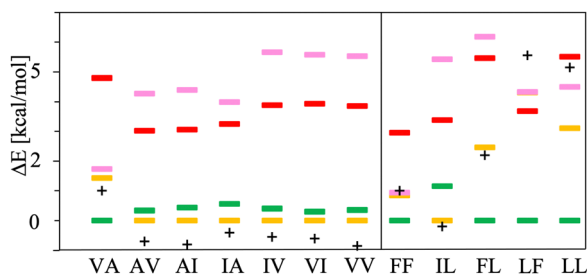


**Fig. 6** Relative energies,  $\Delta E$  in  $\text{kcal mol}^{-1}$ , of the canonical dipeptide conformations in vacuum connected to the *t* (in yellow), *c* (in red), *t'* (in pink) and *c'* (in green) minima along the potential energy surfaces shown in Fig. 5. The reference energy corresponds to the lowest energy conformation found in this work for each system. Left panel class V–A dipeptides. Right panel class F–F dipeptides. For LF, the energy of *t* and *c* conformations is the same, therefore a yellow mark is not distinguishable for this dipeptide. The + symbols stand for the  $\Delta E$  values corresponding to the canonical gas-phase dipeptides reported in ref. 30.

energies for the canonical dipeptides in vacuum investigated by Gonzalez-Diaz *et al.*<sup>30</sup> (the + symbols). As it can be seen, some of these conformations are lower in energy than the ones found here, although by less than  $1 \text{ kcal mol}^{-1}$ . The discrepancy is attributed to the orientation of the  $-\text{COOH}$  capping group. Here it was only sampled for FF, but the ideal orientation may vary depending on the dipeptide and conformation. That may account for the inconsistencies found for VA and IL.

### 3.3. Conformations of dipeptide zwitterions in aqueous solvent

Next, solvation effects are assessed following two steps. First, it is evaluated if structures connected to the energy basins found for the canonical dipeptides in vacuum preserve their

conformation upon transforming them into solvated zwitterions. For that, the structures connected to the minima of each basin are transformed into zwitterions, solvated with explicit solvent and subjected to a md simulation to properly distribute the water molecules around the dipeptide zwitterion (see the methodology section). Then, the solute with a microsolvation shell is extracted from the md trajectories. Such microsolvated dipeptide zwitterions are further fully geometry-optimized using DFT-PBE/TS. The number of water molecules in the microsolvation shells fluctuates between 8 and 13, depending on the dipeptide and the conformation (see Fig. S1 and S2 of the ESI†). The water molecules in the microsolvation shell are chosen such that the backbone amine and carbonyl groups, as well as the charged  $-\text{NH}_3^+$  and  $-\text{COO}^-$  capping groups, form all the expected H-bonds. We have found that after optimization, microsolvated dipeptide geometries change slightly (up to  $20^\circ$  for both  $\phi$  and  $\psi$ ) except for the AV and AI conformers belonging to the *t''* minima. Thus, for most of the dipeptide zwitterions the initial arrangement of their side chains (either *trans* or *cis*) is the same after optimization. For AV and AI, the structures connected to the *t''* minima turned the side chain position into *cis* upon optimization due to changes in  $\phi$  and  $\psi$  around  $40^\circ$ . However, that change is not large enough for considering such structures as part of the *c'* basins. Based on these results one can conclude that solvation and transformation to a zwitterionic state keep the structure in the energetic basin found for the canonical dipeptide in vacuum, and that the conformation, as measured with  $\phi$  and  $\psi$ , changes little, *i.e.*, charged endings in zwitterions do not have a sizable effect on the dipeptide conformation; however, as it is discussed below, they affect the energetic ordering.

In the second step for evaluating the solvation effects, the microsolvation shell of the optimized dipeptide zwitterions is



stripped out. Then, these are solvated with implicit solvent. In this step we have also considered other dipeptide conformations belonging to the *t* and *c* basins, namely the dipeptide zwitterions obtained from the conformations marked with + symbols in Fig. 5. All these structures are fully optimized considering the PCM implicit solvent. Next, the lowest energy conformations found at each basin are chosen for the energy comparison presented in Fig. 7. According to these results, all class V-A PCM-solvated dipeptide zwitterions and some of the class F-F (IL and LL) prefer to adopt a conformation belonging to the *t* basin. The other class F-F PCM-solvated dipeptide zwitterions prefer to adopt conformations belonging to the *c'* basin. Lastly, the PCM-optimized structures are further optimized considering them solvated with the CANDLE implicit solvent model. The energy comparison of the lowest energy conformations found at each basin is presented in Fig. 8. For class V-A, all dipeptide zwitterions prefer to adopt conformations belonging to the *t* basin, as it is found using PCM. However, for class F-F, the outcome is different; all dipeptide zwitterions prefer to adopt conformations belonging to the *c* basin. Differences in the results obtained with PCM and CANDLE are also noticeable in the energetic ordering of the conformations belonging to the other basins. While CANDLE predicts that the second most stable conformation is around 1 to 2 kcal mol<sup>-1</sup> above the most stable ones, PCM predicts differences ranging from 1 to 7 kcal mol<sup>-1</sup>. Moreover, CANDLE predicts that the two lowest energy conformations are connected either to basin *t* or basin *c*, except for LF that prefer basin *c'* for the second lowest energy conformation, whereas PCM predicts that the two lowest energy conformations belong to basin *t*, *c'* or *c*. Yet, both implicit solvation schemes predict that for all dipeptide zwitterions but one (solvated with PCM), the least stable conformation is the connected to the *t'* basin.

It is noteworthy that the lowest energy conformations for all the dipeptide zwitterions solvated with CANDLE, except one, are alike to those observed in their corresponding crystal structures, as is illustrated by the Ramachandran-like plot depicted in Fig. 9. The exception is the conformation for the AV dipeptide, which still belongs to the *t* basin but with a  $\phi$  angle differing about 100° with respect to the experimental value. For that structure, however, an alternative conformation

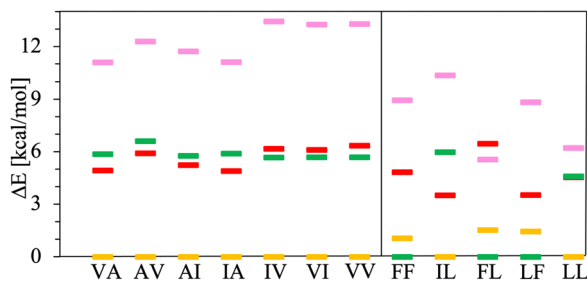


Fig. 7 Relative energies,  $\Delta E$  in kcal mol<sup>-1</sup>, of PCM solvated dipeptide zwitterions. The reference energy corresponds to the lowest energy conformation found in the *t* (in yellow), *c* (in red), *t'* (in pink) and *c'* (in green) basins. Left panel class V-A dipeptides. Right panel class F-F dipeptides.

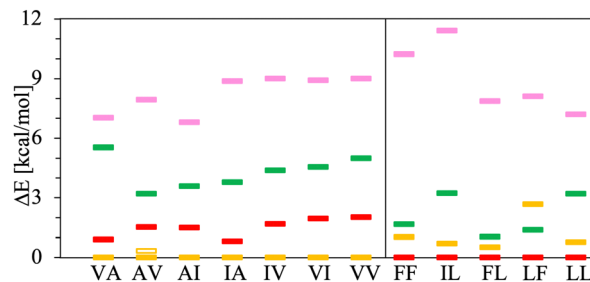


Fig. 8 Relative energies,  $\Delta E$  in kcal mol<sup>-1</sup>, of CANDLE solvated dipeptide zwitterions. The reference energy corresponds to the lowest energy conformation found in the *t* (in yellow), *c* (in red), *t'* (in pink) and *c'* (in green) basins. The yellow open box stands for an alternative conformation found for the AV dipeptide zwitterion in the *t* basin. Left panel class V-A dipeptides. Right panel class F-F dipeptides.

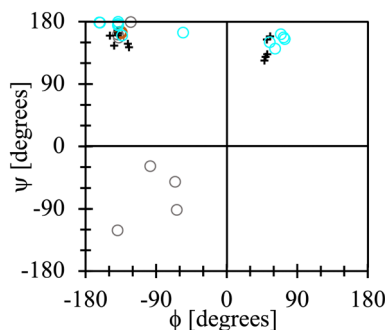


Fig. 9 Lowest-energy dipeptide zwitterion conformations found using the PCM implicit solvent (grey open dots), the CANDLE implicit solvent (cyan open dots) and the dipeptide zwitterion conformations in their crystal structures ("+" symbols). Brown open dot (barely visible) stands for the alternative conformation in the *t* basin for the AV dipeptide zwitterion.

is found in the *t* basin that is solely  $\sim 0.3$  kcal mol<sup>-1</sup> higher in energy than the lowest one (see Fig. 8). This second structure has a  $\phi$  angle that differs by less than 20° from the  $\phi$  value for the dipeptide zwitterion in the crystal structure (brown open dot in Fig. 9).

According to the results presented above, the CANDLE solvation scheme is the one that predicts accurately the tautomerization free energy for glycine. Hence, one may assume that it also correctly describes class V-A and F-F dipeptide zwitterions in aqueous solvent. The latter is supported by our findings about the most stable dipeptide conformations in aqueous solvent, *i.e.*, the CANDLE-solvated dipeptide zwitterions prefer conformations similar to the ones in their corresponding crystal structures.

These results suggest that along the self-assembling path for these systems, the dipeptide zwitterions behave like semi-rigid objects in aqueous solvents, changing little their backbone conformation and side chains relative orientations, thus avoiding large conformational changes that could prevent them from crystallizing in a reasonable time. Therefore, it can be suggested that diffusion and desolvation, but not the conformational changes, should play a major role in the self-assembly process of such systems.

## 4. Conclusions

In this work, we have presented evidence indicating that PBE plus van der Waals corrections, together with the implicit solvent CANDLE adequately describes zwitterions in aqueous solutions. Particularly, the  $\Delta G$  of the tautomerization reaction of Gly in aqueous solvent is accurately predicted, and it is shown that the twelve dipeptide zwitterions resulting from combining Ala, Ile, Leu, Val and Phe hydrophobic amino acids adopt a conformation in aqueous solvent quite similar to that in their corresponding crystal structures. Therefore, it can be suggested that the process that leads to the formation of the corresponding crystal structures involves an assembly of semi rigid objects, which may ease the crystallization of such dipeptide zwitterions from aqueous solutions.

## Conflicts of interest

There are no conflicts to declare.

## Acknowledgements

The authors thank LANCAD and CONACTY for the computer time granted on the supercomputer Yoltla at the LSVP at UAM-Iztapalapa. J. I. acknowledges funding from CONACYT project A1-S-42775 and 1561802. F. A.-C. acknowledges funding from ANID FONDECYT Postdoctorado 2018 no. 3180193 and ANID Convocatoria Nacional Subvención a Instalación en la Academia, Convocatoria año 2021, Folio SA772100091.

## Notes and references

- 1 C. H. Gorbitz, *Chem. – Eur. J.*, 2007, **13**, 1022–1031.
- 2 C. Yuan, W. Ji, R. Xing, J. Li, E. Gazit and X. Yan, *Nat. Rev. Chem.*, 2019, **3**, 567–588.
- 3 M. Monti, E. Scarel, A. Hassanali, M. Stener and S. Marchesan, *Chem. Commun.*, 2023, **59**, 10948–10951.
- 4 C. H. Gorbitz, *Chem. Commun.*, 2006, 2332–2334.
- 5 S. Brahmachari, Z. A. Arnon, A. Frydman-Marom, E. Gazit and L. Adler-Abramovich, *ACS Nano*, 2017, **11**, 5960–5969.
- 6 D. Selkoe, *Nature*, 2003, **426**, 900–904.
- 7 A. Kholkin, N. Amdursky, I. Bdiin, E. Gazit and G. Rosenman, *ACS Nano*, 2010, **4**, 610–614.
- 8 Q. Li, Y. Jia, L. Dai, Y. Yang and J. Li, *ACS Nano*, 2015, **9**, 2689–2695.
- 9 N. Kol, L. Adler-Abramovich, D. Barlam, R. Shneck, E. Gazit and I. Rouso, *Nano Lett.*, 2005, **5**, 1343–1346.
- 10 L. Adler-Abramovich and E. Gazit, *Chem. Soc. Rev.*, 2014, **43**, 6881–6893.
- 11 J. M. del Campo and J. Ireta, *Phys. Chem. Chem. Phys.*, 2021, **23**, 11931–11936.
- 12 J. G. Fernandez and S. Dritsas, *Matter*, 2020, **2**, 1352–1355.
- 13 S. Gupta, I. Singh, A. K. Sharma and P. Kumar, *Front. Bioeng. Biotechnol.*, 2020, **8**, 504.
- 14 C. H. Gorbitz, *Acta Crystallogr., Sect. B: Struct. Sci., Cryst. Eng. Mater.*, 2018, **74**, 311–318.
- 15 J. L. Alonso and J. C. Lopez, in *Gas-Phase IR Spectroscopy and Structure of Biological Molecules*, 2015, vol. 364, pp. 335–401.
- 16 J. Hermans, *Proc. Natl. Acad. Sci. U. S. A.*, 2011, **108**, 3095–3096.
- 17 J. Carlos Campini, M. A. Aguilar and M. Elena Martina, *J. Mol. Liq.*, 2022, **351**, 118557.
- 18 K. Cai, F. Du, J. Liu and T. Su, *Spectrochim. Acta, Part A*, 2015, **137**, 701–710.
- 19 M. Feig, *J. Chem. Theory Comput.*, 2008, **4**, 1555–1564.
- 20 J. Rubio-Martinez, M. Santos Tomas and J. J. Perez, *J. Mol. Graph. Model.*, 2017, **78**, 118–128.
- 21 D. Chakraborty, A. Banerjee and D. J. Wales, *J. Phys. Chem. B*, 2021, **125**, 5809–5822.
- 22 V. Mironov, Y. Alexeev, V. K. Mulligan and D. G. Fedorov, *J. Comput. Chem.*, 2019, **40**, 297–309.
- 23 V. Parchansky, J. Kapitan, J. Kaminsky, J. Sebestik and P. Bour, *J. Phys. Chem. Lett.*, 2013, **4**, 2763–2768.
- 24 R. Vargas, J. Garza, B. Hay and D. Dixon, *J. Phys. Chem. A*, 2002, **106**, 3213–3218.
- 25 F. Carrascoza, S. Zaric and R. Silaghi-Dumitrescu, *J. Mol. Graph. Model.*, 2014, **50**, 125–133.
- 26 F. Adasme-Carreno, J. Caballero and J. Ireta, *J. Chem. Inf. Model.*, 2021, **61**, 1789–1800.
- 27 J. Ireta, *J. Chem. Theory Comput.*, 2011, **7**, 2630–2637.
- 28 C. Cabezas, M. Varela, V. Cortijo, A. I. Jimenez, I. Pena, A. M. Daly, J. C. Lopez, C. Cativiela and J. L. Alonso, *Phys. Chem. Chem. Phys.*, 2013, **15**, 2580–2585.
- 29 C. M. Leavitt, K. B. Moore, III, P. L. Raston, J. Agarwal, G. H. Moody, C. C. Shirley, H. F. Schaefer, III and G. E. Douberly, *J. Phys. Chem. A*, 2014, **118**, 9692–9700.
- 30 N. E. Gonzalez-Diaz, R. Lopez-Rendon and J. Ireta, *J. Phys. Chem. C*, 2019, **123**, 2526–2532.
- 31 S. Lovell, I. Davis, W. Adrendall, P. de Bakker, J. Word, M. Prisant, J. Richardson and D. Richardson, *Proteins*, 2003, **50**, 437–450.
- 32 C. Gorbitz, *Chem. – Eur. J.*, 2001, **7**, 5153–5159.
- 33 C. Gorbitz, *New J. Chem.*, 2003, **27**, 1789–1793.
- 34 J. Wang, K. Liu, R. Xing and X. Yan, *Chem. Soc. Rev.*, 2016, **45**, 5589–5604.
- 35 Z. Chaker, P. Chervy, Y. Boulard, S. Bressanelli, P. Retailleau, M. Paternostre and T. Charpentier, *J. Phys. Chem. B*, 2021, **125**, 9454–9466.
- 36 E. Mayans and C. Alemán, *Molecules*, 2020, **25**, 6037.
- 37 T. O. Mason, D. Y. Chirgadze, A. Levin, L. Adler-Abramovich, E. Gazit, T. P. J. Knowles and A. K. Buell, *ACS Nano*, 2014, **8**, 1243–1253.
- 38 D. G. Fedorov, *J. Chem. Theory Comput.*, 2019, **15**, 5404–5416.
- 39 C. M. Aikens and M. S. Gordon, *J. Am. Chem. Soc.*, 2006, **128**, 12835–12850.
- 40 R. Tripathi, L. Durán Caballero, R. Pérez de Tudela, C. Hölzl and D. Marx, *ACS Omega*, 2021, **6**, 12676–12683.
- 41 J. Ireta, *Int. J. Quantum Chem.*, 2012, **112**, 3612–3617.
- 42 J. Ireta, *Theor. Chem. Acc.*, 2016, **135**, 220.
- 43 R. Sundararaman and W. A. Goddard, III, *J. Chem. Phys.*, 2015, **142**, 064107.





- 44 A. Fortunelli and J. Tomasi, *Chem. Phys. Lett.*, 1994, **231**, 34–39.
- 45 V. Barone, M. Cossi and J. Tomasi, *J. Chem. Phys.*, 1997, **107**, 3210–3221.
- 46 J. Tomasi, B. Mennucci and R. Cammi, *Chem. Rev.*, 2005, **105**, 2999–3094.
- 47 J. P. Perdew, K. Burke and M. Ernzerhof, *Phys. Rev. Lett.*, 1996, **77**, 3865–3868.
- 48 S. Grimme, *J. Comput. Chem.*, 2006, **27**, 1787–1799.
- 49 A. V. Marenich, C. J. Cramer and D. G. Truhlar, *J. Phys. Chem. B*, 2009, **113**, 6378–6396.
- 50 S. A. Petrosyan, J.-F. Briere, D. Roundy and T. A. Arias, *Phys. Rev. B: Condens. Matter Mater. Phys.*, 2007, **75**, 205105.
- 51 D. Gunceler, K. Letchworth-Weaver, R. Sundararaman, K. A. Schwarz and T. A. Arias, *Model. Simul. Mater. Sci. Eng.*, 2013, **21**, 074005.
- 52 R. Sundararaman, K. A. Schwarz, K. Letchworth-Weaver and T. A. Arias, *J. Chem. Phys.*, 2015, **142**, 054102.
- 53 R. Sundararaman and T. Arias, *Comput. Phys. Commun.*, 2014, **185**, 818–825.
- 54 M. J. Frisch, G. W. Trucks, H. B. Schlegel, G. E. Scuseria, M. A. Robb, J. R. Cheeseman, G. Scalmani, V. Barone, B. Mennucci, G. A. Petersson, H. Nakatsuji, M. Caricato, X. Li, H. P. Hratchian, A. F. Izmaylov, J. Bloino, G. Zheng, J. L. Sonnenberg, M. Hada, M. Ehara, K. Toyota, R. Fukuda, J. Hasegawa, M. Ishida, T. Nakajima, Y. Honda, O. Kitao, H. Nakai, T. Vreven, J. A. Montgomery, Jr., J. E. Peralta, F. Ogliaro, M. Bearpark, J. J. Heyd, E. Brothers, K. N. Kudin, V. N. Staroverov, R. Kobayashi, J. Normand, K. Raghavachari, A. Rendell, J. C. Burant, S. S. Iyengar, J. Tomasi, M. Cossi, N. Rega, J. M. Millam, M. Klene, J. E. Knox, J. B. Cross, V. Bakken, C. Adamo, J. Jaramillo, R. Gomperts, R. E. Stratmann, O. Yazyev, A. J. Austin, R. Cammi, C. Pomelli, J. W. Ochterski, R. L. Martin, K. Morokuma, V. G. Zakrzewski, G. A. Voth, P. Salvador, J. J. Dannenberg, S. Dapprich, A. D. Daniels, Ö. Farkas, J. B. Foresman, J. V. Ortiz, J. Cioslowski and D. J. Fox, *Gaussian 09 Revision E.01*, Gaussian Inc., Wallingford, CT, 2009.
- 55 R. Sundararaman, K. Letchworth-Weaver, K. A. Schwarz, D. Gunceler, Y. Ozhabes and T. Arias, *SoftwareX*, 2017, **6**, 278–284.
- 56 K. F. Garrity, J. W. Bennett, K. M. Rabe and D. Vanderbilt, *Comput. Mater. Sci.*, 2014, **81**, 446–452.
- 57 A. Tkatchenko and M. Scheffler, *Phys. Rev. Lett.*, 2009, **102**, 073005.
- 58 J. Nochebuena, A. Ramirez and J. Ireta, *Int. J. Quantum Chem.*, 2015, **115**, 1613–1620.
- 59 P. Blöchl, *Phys. Rev. B: Condens. Matter Mater. Phys.*, 1994, **50**, 17953–17979.
- 60 G. Kresse and D. Joubert, *Phys. Rev. B: Condens. Matter Mater. Phys.*, 1999, **59**, 1758–1775.
- 61 G. Kresse and J. Furthmüller, *Phys. Rev. B: Condens. Matter Mater. Phys.*, 1996, **54**, 11169–11186.
- 62 P. Pulay, *Chem. Phys. Lett.*, 1980, **73**, 393–398.
- 63 W. Humphrey, A. Dalke and K. Schulten, *J. Mol. Graph.*, 1996, **14**, 33–38.
- 64 J. Huang and A. D. MacKerell Jr, *J. Comput. Chem.*, 2013, **34**, 2135–2145.
- 65 W. L. Jorgensen, J. Chandrasekhar, J. D. Madura, R. W. Impey and M. L. Klein, *J. Chem. Phys.*, 1983, **79**, 926–935.
- 66 U. Essmann, L. Perera, M. L. Berkowitz, T. Darden, H. Lee and L. G. Pedersen, *J. Chem. Phys.*, 1995, **103**, 8577–8593.
- 67 S. Miyamoto and P. A. Kollman, *J. Comput. Chem.*, 1992, **13**, 952–962.
- 68 J.-P. Ryckaert, G. Ciccotti and H. J. Berendsen, *J. Comput. Phys.*, 1977, **23**, 327–341.
- 69 G. J. Martyna, D. J. Tobias and M. L. Klein, *J. Chem. Phys.*, 1994, **101**, 4177–4189.
- 70 S. E. Feller, Y. Zhang, R. W. Pastor and B. R. Brooks, *J. Chem. Phys.*, 1995, **103**, 4613–4621.
- 71 J. C. Phillips, D. J. Hardy, J. D. Maia, J. E. Stone, J. V. Ribeiro, R. C. Bernardi, R. Buch, G. Fiorin, J. Hénin and W. Jiang, *et al.*, *J. Chem. Phys.*, 2020, **153**, 044130.
- 72 J. T. Edsall and M. H. Blanchard, *J. Am. Chem. Soc.*, 1933, **55**, 2337–2353.
- 73 G. Wada, E. Tamura, M. Okina and M. Nakamura, *Bull. Chem. Soc. Jpn.*, 1982, **55**, 3064–3067.
- 74 J. H. Jensen and M. S. Gordon, *J. Am. Chem. Soc.*, 1995, **117**, 8159–8170.
- 75 Y. Ding and K. Krogh-Jespersen, *J. Comput. Chem.*, 1996, **17**, 338–349.
- 76 O. Rahaman, A. C. T. van Duin, W. A. Goddard and D. J. Doren, *J. Phys. Chem. B*, 2011, **115**, 249–261.
- 77 W. Tang, C. Cai, S. Zhao and H. Liu, *J. Phys. Chem. C*, 2018, **122**, 20745–20754.
- 78 O. Andreussi, I. Dabo and N. Marzari, *J. Chem. Phys.*, 2012, **136**, 064102.
- 79 C. Dupont, O. Andreussi and N. Marzari, *J. Chem. Phys.*, 2013, **139**, 214110.
- 80 G. N. Ramachandran, C. Ramakrishnan and V. Sasisekharan, *J. Mol. Biol.*, 1963, **7**, 95–99.

